MICROSTRUCTURE AND MECHANICAL PROPERTIES OF SS 316L – CNT METAL MATRIX COMPOSITE FABRICATED BY METAL INJECTION MOLDING PROCESS

Thota Siva Prasad[1*], C. Yuvaraj[2], K. Prahlada Rao[3]

Abstract

The Metal Injection Molding (MIM) technique was employed to fabricate components utilizing a composition of SS 316L – CNT metal matrix composites, combining SS 316L and Carbon NanoTubes. A thorough investigation was conducted to assess the influence of varying sintering parameters on resultant microstructures and mechanical properties, including an analysis of fractographic patterns post-tensile testing. The outcomes unveiled effective densification within the temperature window of 1120–1175 ◦C during vacuum sintering. Excessive temperature or prolonged sintering durations led to challenges such as distortion, sintered body warping, or coarsening of lamellar colonies. Through judicious sintering parameter selection (1175 ◦C, 2 h), a composite material attaining a relative density of 96.2% was achieved. The microstructure showcased a uniform and finely-grained lamellar architecture, with α2/γ lamellar colonies averaging 60 μm in dimension, showcasing limited β phase presence alongside scarce carbon nanotube precipitates. Mechanical attributes encompassed a compressive strength of 283 MPa, a compressibility measure of 34.9%, an ultimate tensile strength of 482 MPa, and a plastic elongation of 0.46%. Tensile tests predominantly illuminated translamellar fracture patterns, with microcracks frequently originating from pore sites and interfaces between SS 316L and carbon nanotubes.

[1*]Research Scholar, Department of Mechanical Engineering, Jawaharlal Nehru Technological University Anantapuramu.
[2]Professor & Principal, Department of Mechanical Engineering, Madanapalle Institute of Technology & Science, Madanapalle
[3]Professor, Department of Mechanical Engineering, Jawaharlal Nehru Technological University Anantapuramu

***Corresponding author:-** Thota Siva Prasad
Research Scholar, Department of Mechanical Engineering, Jawaharlal Nehru Technological University Anantapuramu.Email Id:- thotasivaprasad2004@gmail.com

DOI: 10.48047/ecb/2023.12.si10.00389

1. Introduction

Steel-based composites have garnered significant interest and have been utilized in both structural and engine components of automobiles due to their advantageous attributes, including low density, remarkable high-temperature strength, and resistance to oxidation [1–3]. More recently, Carbon nanotubes (CNTs) have emerged as crucial and effective additives for enhancing mechanical properties, particularly high-temperature strength, in SS 316L. Composites featuring high concentrations of CNTs are being considered as potential materials for high-temperature structural applications [4,5]. However, these composites exhibit reduced ductility and toughness at room temperature, and the inclusion of substantial amounts of CNTs introduces challenges in their fabrication [6,7]. Traditionally, these composites have been produced using ingot metallurgy methods [8,9]. Nonetheless, the limited ductility at room temperature poses difficulties for subsequent conventional manufacturing processes, especially when crafting parts with high CNT content in SS 316L composites. Powder metallurgy (PM) techniques offer a more appealing approach, enabling a high degree of chemical homogeneity and mitigating macroscopic segregations. Among these techniques, the Metal Injection Molding (MIM) process stands out as a net-shape powder metallurgy forming method that proves cost-effective for the mass production of intricate, precision parts [10–12]. In this particular investigation, the MIM process was employed for fabricating parts composed of SS 316L composites containing CNTs. The study focused on identifying suitable injection molding process variables, particularly optimal sintering parameters. The research delved into the impact of sintering temperature and time on the resulting microstructures and mechanical properties of the composites. Additionally, an analysis of the fractographic features subsequent to tensile tests was conducted [22].

Steel-based composites have garnered substantial attention, finding utility in both structural and engine components of automobiles, thanks to their inherent advantages, including low density, exceptional high-temperature strength, and resistance to oxidation [1–3]. In recent times, Carbon nanotubes (CNTs) have emerged as indispensable additives, significantly enhancing the mechanical attributes, particularly high-temperature strength, of SS 316L. These composites, with elevated CNT concentrations, hold promise as potential materials for high-temperature structural applications [4,5]. Nevertheless, it is noteworthy that these commendable enhancements often accompany a trade-off in ductility and toughness at room temperature, compounded by the challenges arising from the incorporation of substantial CNT quantities in fabrication processes [6,7].

Historically, the realm of these composites has been shaped by the crucible of ingot metallurgy methods [8,9]. Nonetheless, the inherent limitation in room temperature ductility introduces complexities, especially when traversing conventional manufacturing routes, particularly for parts infused with a substantial CNT quotient in SS 316L composites. Enter the stage, Powder Metallurgy (PM) techniques, an alluring avenue that beckons, fostering a realm of chemical homogeneity and attenuating macroscopic disparities. Within this tapestry of techniques, the Metal Injection Molding (MIM) process shines as a beacon a net-shape powder metallurgy forging, bearing the mantle of cost effectiveness for mass-producing intricate, precision-driven components [10–12].

Within this very exploration, the MIM process unfurled its wings, a virtuoso orchestrating the creation of SS 316L composites adorned with the presence of CNTs. The heart of this endeavor pulsated to the rhythm of optimal sintering parameters, seeking to unearth the ideal confluence of variables within the injection molding process. The spotlight of inquiry danced upon the threshold of sintering temperature and duration, an intimate tango poised to sculpt microstructures and mechanical attributes within these composites. And, as the crescendo of tensile tests subsided, a reverent analysis unveiled the fractographic tapestry, a testament to the journey undertaken a tale etched upon the canvas of materials and process variables, within the realm of SS 316L-CNT composites

2. Experimentation of SS 316L

2.1 Raw materials

Composite powders incorporating Carbon Nano Tubes (CNTs) were meticulously synthesized, with SS 316L powder serving as the foundational matrix (at.%). The initial composition embarked on a journey through the crucible of a dual plasma arc furnace fabrication, a transformative metamorphosis that culminated in annealing at 1200 ◦C for a span of 50 hours an alchemical union intended to weave the fabric of

compositional harmony. The resulting symphony, an ingot steeped in homogeneity, was then sculpted into dimensions of Ø18 mm × 220 mm, a canvas prepared for the artistry yet to unfold. With the stage set, an arcane alchemy known as PIGA (plasma melting induction guiding gas atomization) emerged from the shadows, propelled by argon gas atomization a technique that conjured the ingot into a waltz of composite powder particles. An entrancing ballet unfolded, a dance of transformation rendering particles akin to stardust, each a vessel of potential. These particles, graced by the sieve's discerning embrace, embarked on a classification, a division that yielded particles of finesse, those that slipped through the mesh of a 200-mesh sieve a congregation primed for the ensuing metamorphosis within the embrace of the injection molding process. The canvas of this narrative, imbued with particles' essence, unfurls a tableau in Figure 1, a vista that unfolds the story of predominantly spherical particles, each boasting an average diameter of approximately 50 µm. Minimal satellites dot this cosmic landscape, a testament to the precision of the process's artistic rendering. It is within this morphology, this celestial dance of form, that lies the key a key unlocking the gates to the Metal Injection Molding (MIM) process, where these particles shall find their purpose, a symphony of transformation orchestrated upon the grand stage of fabrication.

2.2 MIM process

Details of the fabrication and the parameters in MIM process were given as follows:

In the realm of feedstock preparation, an exquisite dance of elements transpires a choreography of composite powder and binder, orchestrated with meticulous precision at a designated ratio. The alchemical amalgam unfurls its tale, SS 316L and CNT powder composite converging, their embrace enhanced by a binder symphony 63% (wt.%) Paraffin Wax (PW), 20% (wt.%) High Density Polyethylene (HDPE), and 12% (wt.%) Stearic Acid (SA) a harmonious composition deemed optimal through discerning eyes. The symphony of properties and rheological attributes intertwines, a nexus guiding the hand towards a selection 65% powder loading, the chosen embodiment of potential. With reverence, the chosen feedstock emerges, the melding of powder and binder, an artful fusion unveiled within the embrace of a custom twin-blade, horizontal-axis mixing apparatus. At a temperature of 210 ◦C, this union unfolds, a 30-minute symposium of melding, a transformative alchemy giving birth to a feedstock poised to partake in the grand tapestry of creation.

The domain of injection molding unfurled its canvas, a theater where innovation takes form. A standard plastic injection molding machine donned the role of an artist, shaping injection compacts with deft precision. Within its embrace, intricate contours intertwined with cuboidal essence, a symphony of shapes, each with dimensions of 35 mm × 20 mm × 6 mm purposefully crafted, a stage for forthcoming tests.

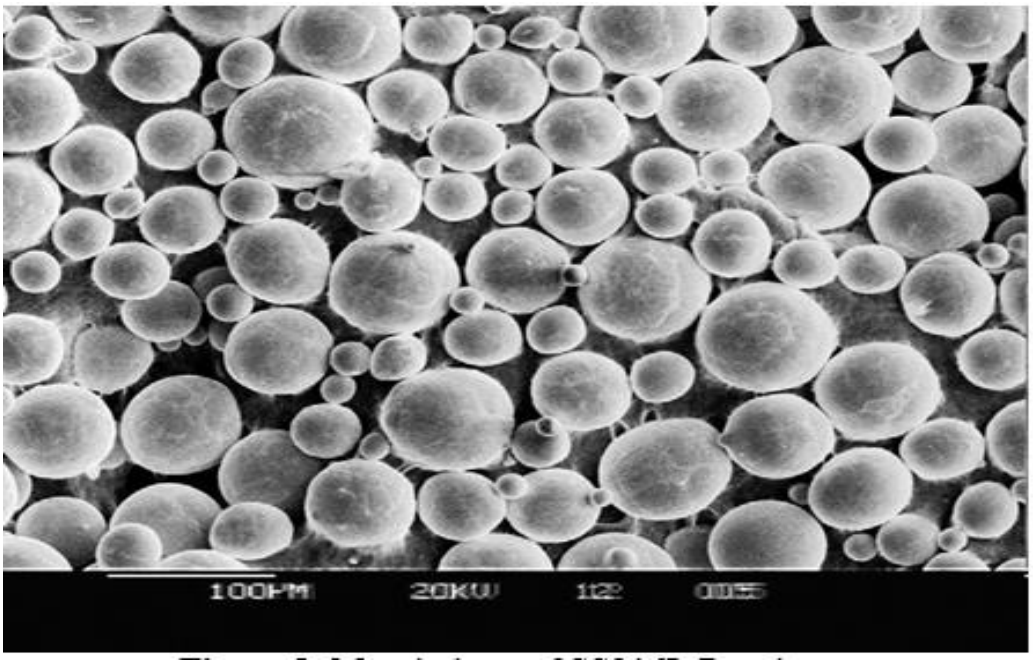

Figure 1. Morphology of SS316L Powder

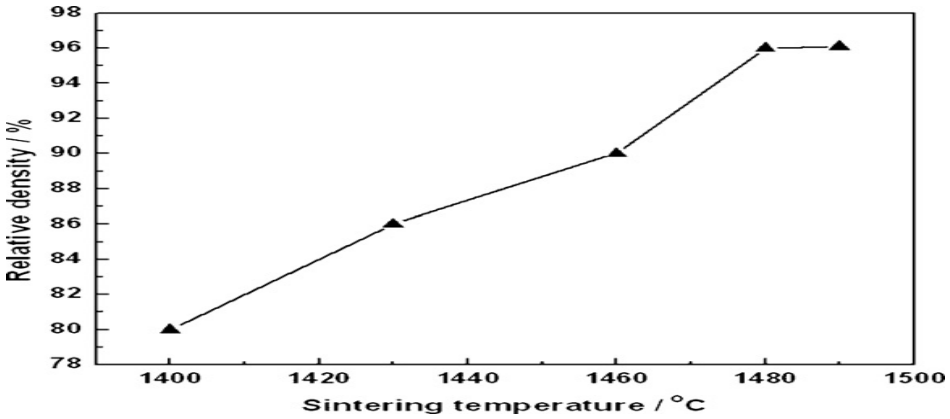

Figure 2. Sintering temperature Vs Relative Density of work specimen

In the crucible of experimentation, a dance of variables commenced—a choreography seeking perfection. The ensemble of pressure, temperature, and mold temperature engaged in a pas de trois, a tango of factors swirling in unison. The script unfolded, revealing that an injection pressure of 90 MPa, a temperature of 150 ◦C for injection, and a mold temperature of 30 ◦C became the triumphant culmination the crescendo of optimal outcomes, etching their mark upon the canvas of the injection process. The journey of debinding unfolds, a delicate two-step ballet, orchestrated by the chosen binder system. Sequential in nature, the process unfurls with precision, a choreography of solvent debinding followed by the embrace of thermal liberation. Solvent debinding commences, a ritual of immersion within a Polypropylene-laden bath, a temperature of 40 ◦C, a reverie spanning 12 hours. Emerging from this aqueous cocoon, the compacts embark upon a 6-hour rendezvous with dryness, a period of transition that sets the stage for the next movement.

The subsequent act unfurls, a symphony of thermal debinding, a crescendo played within the spectrum of 30 to 600 ◦C. The backdrop, a vacuum atmosphere, shrouding the process in an aura of isolation, an environment marked by a pressure of 10^-3 Pa. Here, the bonds of the binder begin their quiet exodus, yielding to the forces of change, yielding to the call of transformation.

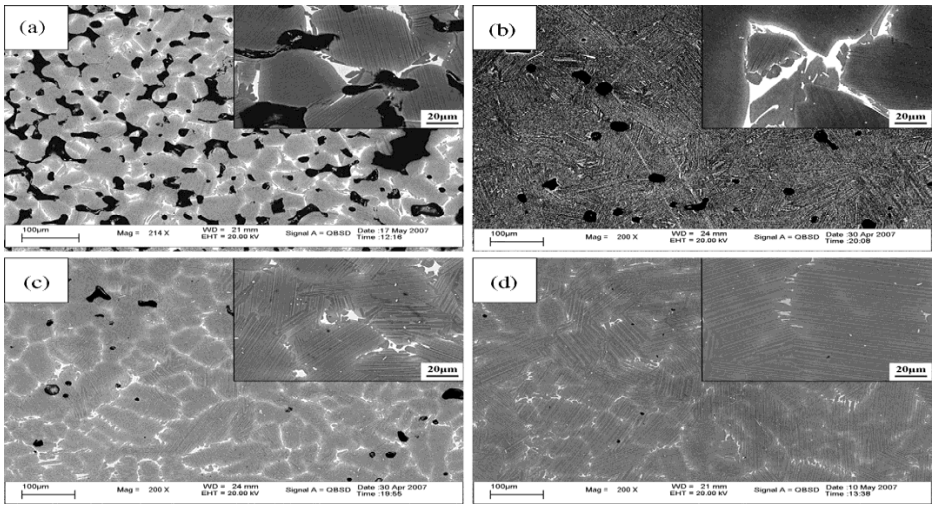

Figure. 3. Microstructures of the Specimens sintered at different temperatures for 1 h: (a) 1120 ◦C; (b) 1140 ◦C; (c) 1160 ◦C; (d) 1175 ◦C.

And then, the stage shifts. Sintering emerges from the wings, a momentous event held within the embrace of a vacuum furnace, bedecked with molybdenum heating elements. The compacts, having traversed the path of debinding, stand at the precipice of metamorphosis. The spectrum of temperature intervals stretches before them, a via from 1400 to 1500 ◦C, a span of time extending from 0.5 to 3 hours for each, a series of intervals that promise to unveil their ultimate form. Within this alchemical crucible, the symphony of sintering unfolds, a symphony composed of temperature, time, and the alchemy of transformation.

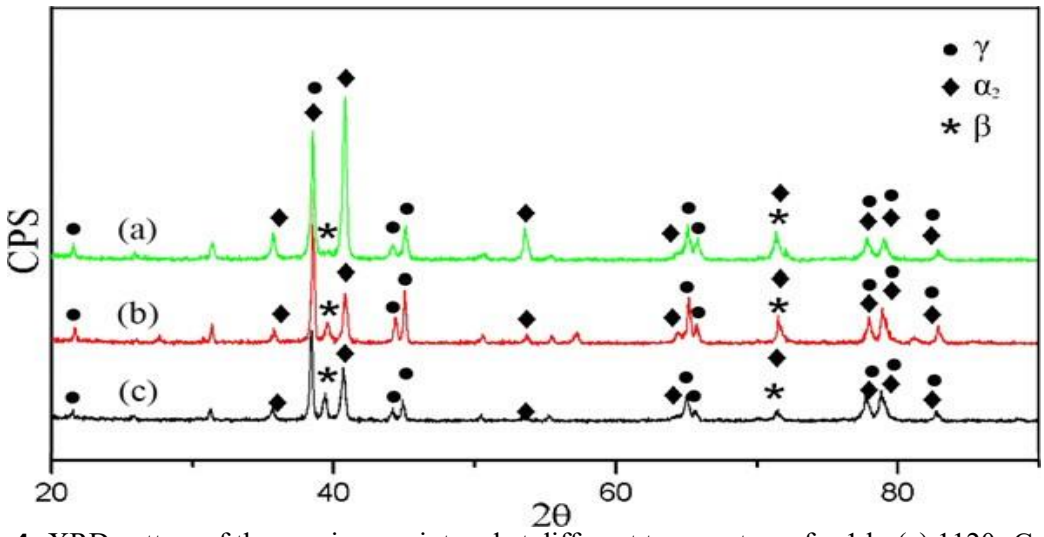

Figure. 4. XRD patters of the specimens sintered at different temperatures for 1 h: (a) 1120 ◦C; (b) 1160 ◦C; (c) 1175◦C.

Table 1. EDS Analysis

Analysis location	SS 316L (at.%)	CNT (at.%)
Lamellar colony	45.49	46.36
β phase	54.72	36.73

2.3 Characterization

Amidst the realm of characterization, a quest for understanding took shape. The densities of specimens unfolded, their secrets unveiled through the enigmatic waters of the underwater gravimetric method. The stage of microstructural exploration beckoned, scanning electron microscopy assuming the role of a maestro, capturing images in backscattered electron (BSE) radiance, accompanied by the harmonies of energy dispersive spectroscopy (EDS), unraveling tales of elemental composition.

Constituent phases emerged from the shadows, unveiled through the symphony of X-ray diffraction (XRD) analysis. In the embrace of a conventional diffractometer, Cu Kα radiation painted a portrait of crystalline composition, unveiling the hidden facets of the materials' essence.

And then, the mechanical arena called, a platform of tension and compression, a theater of tests performed at the ambient embrace of room temperature. The Instron material tester stood vigilant, a conductor of forces and strains. Strain rates of 1 × 10^-3 s^-1 and 5 × 10^-3 s^-1 became the tempo, orchestrating the motions of tensile and compressive evaluations. Spark erosion, a sculptor of form, shaped the specimens into plates and cylindrical columns, each a canvas for the symphony of forces to be played. Within the gauge regions, refinement beckoned, emery paper dancing across the surface, ushering in a refinement of texture and precision. The narrative of material response, of resilience and strength, was etched upon this stage, an intricate tapestry woven by meticulous tests and deliberate preparations.

3. Results And Discussion

3.1 Effect of Sintering Temperature on Microstructure

Behold Figure 2, a visual symphony of relative densities unveiled through the artistic mastery of sintering under vacuum's gaze. An hour of contemplation, a dance of temperatures—this is the narrative inscribed upon this canvas. A crescendo of densification rises, a ballet of transformation painted in varying hues. As the temperature rises, so too does the density, a harmonious progression observed. The stage of effective densification finds its zenith within the realm of 1120–1175 ◦C, a realm where the alchemy of transformation unfolds with utmost grace. A pinnacle of 96% relative density stands tall, a testament to the artistry of sintering at 1175 ◦C. Yet, as the temperatures soar beyond, a subtle equilibrium is achieved, and incremental increments in temperature yield but whispers of change a delicate balance achieved. Turn now to Figure 3, a tapestry woven with microstructural threads. An hour's embrace within the fires of sintering, a journey through the temperature tapestry the outcome, a window into the microcosm. The magnifying lens of X-ray diffraction, as captured in Figure 4, unveils the presence of three distinct actors, three phases in

this grand performance: α2, γ, and β. Each a character in this cosmic play, their presence etched in crystalline harmony, revealing their identities through diffraction's dance. Thus, the narrative unfolds, a saga of densities and microcosms, a symphony of phases and transformations, each figure etching its mark upon the canvas of understanding.

At the crucible of 1100 ◦C, a tale of transformation unfolds in the sintered specimen (Figure 3a). Here, the composite powders meld, forming intimate bonds, their interfaces etched with precision. Pores punctuate this landscape, and the enigmatic β phase stands as a white sentinel along former particle boundaries, casting shadows of intrigue.

Ascend to 1110 ◦C, and the narrative shifts (Figure 3b). Particle interfaces recede from view, their contours fading into obscurity. The β phase assumes a minor role, taking its place discreetly at the triple junctions, a silent observer of the evolving drama. Behold the sintered tableau at 1160 ◦C (Figure 3c), where echoes of transformation reverberate. This mirage finds kinship with its counterpart at 1175 ◦C (Figure 3d). Pores diminish, and lamellar colonies expand, their average size scaling new heights of 60 µm. A symphony of near-lamellar microstructure unfurls at 1175 ◦C, where α2/γ lamellar colonies interplay with the β phase. A choreography of β phase emerges at junctions and boundaries, woven into a reticulate tapestry, a testament to the union of elements. EDS analysis (Table 1) lays bare the secret of the β phase, rich in CNTs, defying the confines of the composite's composite. Boride particles dance in rod-like formations, and yttrium oxide precipitates embellish this microcosm, revealing their identities under the watchful gaze of SEM-BSE images (Figure 5). Delve further into their stories within SS 316L-CNT composites in the annals of existing literature [14–17].

Figure 6 unveils the creations of the MIM process composite components of intricate geometries, born from the fires of creativity. Yet, tread cautiously beyond 1175 ◦C, for there lies a realm of distortion and warping, a tale of the incomplete homogeneity of composition. Excessive temperatures kindle localized melting, sowing seeds of distortion and liquid phase extravagance. 1175 ◦C emerges as the Goldilocks of sintering, crafting a near-lamellar masterpiece, where α2/γ lamellar colonies thrive in harmonious abundance. In comparison to as-cast ingots, marred by the scars of segregation and L-shaped patterns, the MIM composite beckons with a promise of unity (Figure 7). A symphony of homogeneity graces its microstructure, a tapestry woven with finer threads, a sanctuary free of macroscopic segregations. Herein lies the alchemy of transformation, where the journey from composite powders to intricate structures is etched with the finesse of precision, and material properties ascend to new heights.

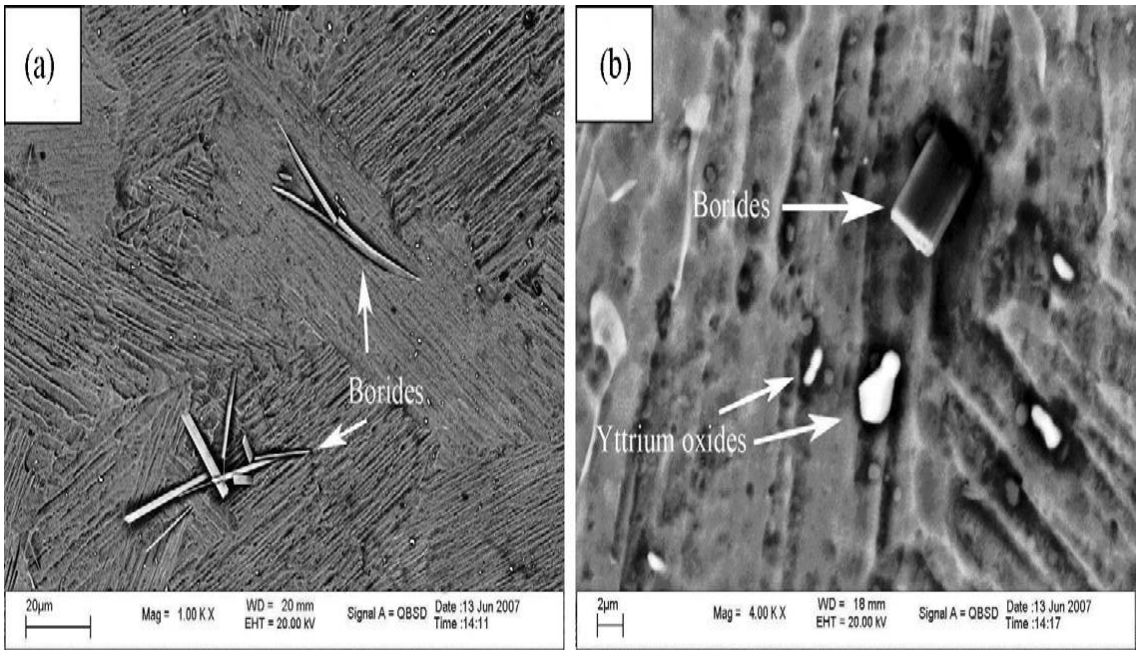

Figure. 5. SEM morphologies of carbon nano tubes in the etched specimens:

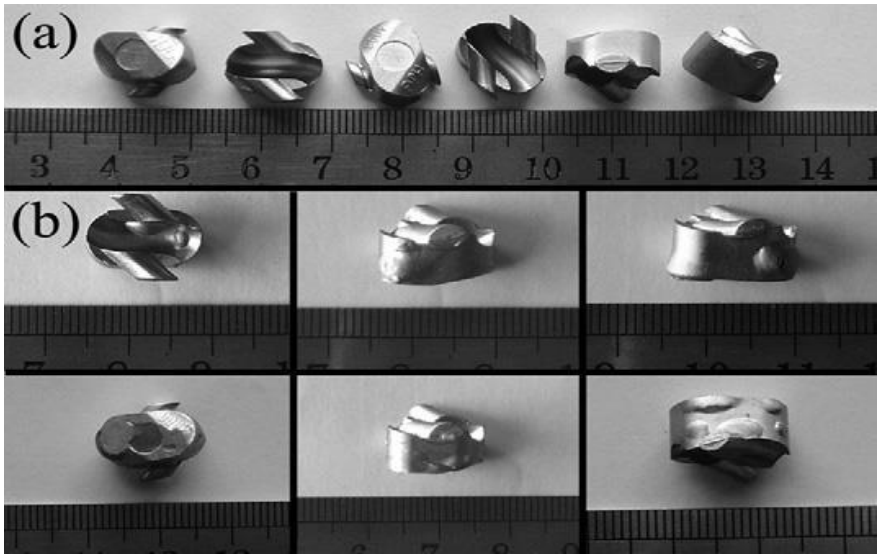

Figure. 6. Pictures of SS 316L-CNT composite parts with complex shapes fabricated by MIM process: (a) sintered at 1175 ◦C; (b) sintered at 1180 ◦C (above three) or 1200 ◦C (below three).

3.2 Effect of Sintering Time on Microstructure

From Fig. 7 shows the relative densities of the specimens sintered in vacuum at 1175 ◦C for different times. The relative density of the sintered specimen at 1175 ◦C for 0.5 h was a lower value of 93.1%.

Subsequent stages saw the relative density of specimens soar with urgency, culminating at a resolute 96% at the zenith of 1175 ◦C, a testament to the culmination of their transformation through the crucible of sintering. A venture into prolonged sintering, spanning 2 hours or 3 hours, unveiled only meager gains in relative density—an incremental ascent to 96.2% and 96.3%, a whisper of improvement beyond the orchestration of 1 hour. With such revelations, the curtain was drawn on the notion that extending sintering time alone could usher in the realm of full density.

As the sands of time trickled, microstructures unfurled, a tableau of near-lamellar symphony, a convergence of α2/γ lamellar colonies clad in variations of β phase and lamellar garb. Figure 8 emerges, each frame narrating a unique tale within the tapestry of sintering durations.

At the dawn of 1175◦C, the hourglass of transformation revealed a spectacle (Figure 8a), akin to its sibling sintered for 1 hour (Figure 8b). Yet, beneath the surface, the former bore a heavier burden of pores, while the chorus of lamellar colonies maintained their harmonious average size of 50 μm. With the passage of 2 hours, the symphony took a new turn (Figure 8c). The reticulate β phase morphed, evolving into whispers of α2 and γ phases. In this transformation, a dance of homogeneity played out, a testament to the alchemy within the sintered body. And the chorus of lamellar colonies stood unwavering in their arrangement.

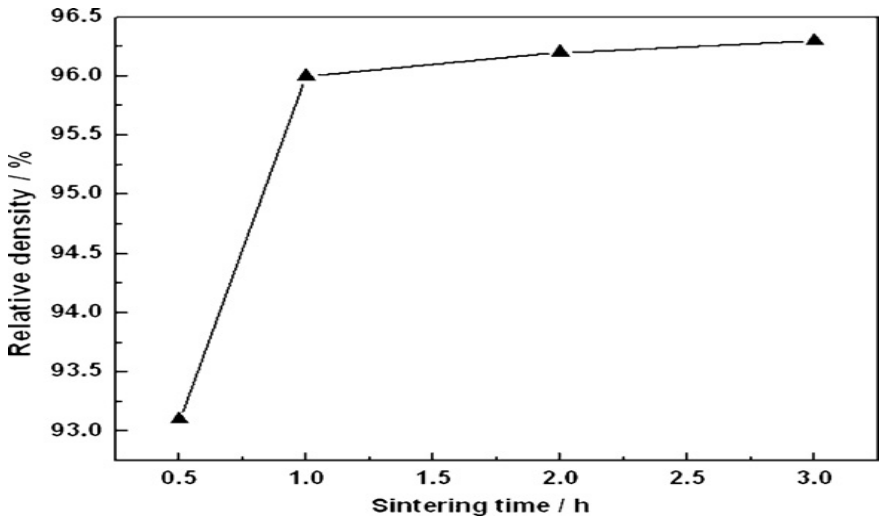

Figure 7. Relationship between relative density and sintering time.

Table 2 EDS analysis

Analysis location	SS 316L (at.%)	CNT (at.%)
Lamellar colony	45.35	44.56
Black region	46.89	44.34

Behold, in the gallery of time, the chronicle of 3 hours (Figure 8d), a story unfolding in shades of white and black. The once-reticulate β phase took a bow, assuming a new guise of nubbly segregation, as if in homage to its former self. Amid the lamellar colonies, distinctive black forms emerged, a symphony of shapes curved and bound by the boundaries of their existence. The veil of EDS analysis lifts, revealing the inner secrets of Table 2, where revelations unfurl like chapters in an ancient tome. The enigmatic black regions, cloaked in mystery, harbor a greater affinity for SS 316L, boasting a presence of around 3%, while the CNTs retreat to the shadows, whispering their secrets in lower concentrations compared to the lamellar colonies. This spectral dance of elements echoes the haunting refrain of S-segregation, a symphony sung by other researchers in the archives of as-cast composites [19].

Yet, amid the orchestra of transformations, a protagonist emerges the lamellar colonies. In the realm of the 3-hour sintered specimen, they undergo a metamorphosis, a coarsening, their once-timid forms swelling to an average size of 200 µm, a testament to the passage of time and the alchemy of the furnace. And in this grand transformation, the boride rods and the ethereal yttrium oxide particles refuse to fade, their presence an ode to resilience within the crucible of change. Thus, with a resolute gaze into the heart of the composite, we lay down our quills, a conclusion etched in the annals of understanding 1175 ◦C for the span of 2 hours, the perfect crucible for the birth of the optimal SS 316L microcosm.

3.3 Mechanical Properties

The annals of our exploration lay bare the essence of strength, revealed through the trials of compressive and tensile tests, each specimen a testament to the crucible of sintering. Behold Table 3, a tapestry woven from the threads of data, where the specimen sintered at 1480 ◦C for 2 hours emerges as the sovereign, donning the mantle of superior properties. A symphony of strengths and strains unfolds, a choreography orchestrated by microstructure—those voids and pores reduced, grain size finer. Within this intricate dance, a tale of contrasts unfolds, where compressive strength reigns, standing tall at 6 to 8 times the Ultimate Tensile Strength (UTS), while compressive strain stretches its arms, spanning 50 to 60 times the realm of tensile strain. Such a narrative, a tribute to the brittleness of our SS 316L-based creation. Tensile loading, a precursor to the elegy of micro cracks, unfurls the drama of propagation driven by tensile stress, a relentless march towards demise. Yet, under the embrace of compressive forces, micro cracks may stir, but their advance remains constrained, their ambitions curtailed. Yet, amidst the verses of strength, a shadow of disparity looms, a stark contrast to the tales of yore. The values of Ultimate Tensile Strength (UTS) and strain (ε), though etched in the parchment of MIM composites' microstructure, bow humbly to their as-cast counterparts, their echoes faint. A riddle unsolved, this divergence, perhaps a tribute to the whisper of porosity, the specter of oxygen. A reminder that even as we forge anew, the echoes of the past linger, shaping the destiny of strength and resilience.

Let us cast our gaze upon the specimen sintered at 1480 ◦C for 2 hours, a creation of meticulous craftsmanship, yet harboring subtle shadows. Within its crystalline tapestry, a story unfolds of porosity, oxygen, and the enigma they weave. Behold, approximately 4% porosity and a curious embrace of around 1800 ppm oxygen content grace this specimen, numbers that stand higher than the echoes of the as-cast counterparts [9]. A conundrum, unravelled when the MIM process takes the stage. As the curtain rises, the initial composite powders, nimble wanderers, traverse a path fraught with risks, where oxygen and the binder system leave their imprint during the dance of feedstock preparation, debinding, and sintering. Yet, let us delve deeper into this saga of oxygen, for within its embrace, lies a tale of transformation. The α2 (SS 316L) and γ (SS 316L) phases, bedfellows to oxygen's waltz, endure a metamorphosis, embarking upon a journey of embrittlement. The very fabric of the MIM composite, woven with care, bears the imprint of this elemental interlude.

A call to arms emerges from these whispers of oxygen, an ode to the realm of possibilities. Envision a symphony where mechanical prowess reigns supreme, where oxygen's grasp is

relinquished, and the symphony of flaws finds its crescendo. As the baton is passed, it is believed that the mechanical prowess of MIM composites shall rise, unfettered, an evolution marked by the alchemy of minimizing oxygen's touch and breathing life into a world devoid of material flaws.

A noteworthy observation graces the realm of fracture surfaces, where the intricate dance of boride rods and strip-shaped segregations of the β phase unfolds. A tale told by the A and B arrows in Figures 10a and c, etching a narrative upon the canvas of failure. A quest for understanding led us to wield the tool of EDS analysis, and its revelations are inscribed within the annals of Table 4.

Among the artifacts, a singular figure emerges the boride rod, a traveler plucked from the heart of the material matrix in the throes of failure. Its departure left behind an indelible mark, an indentation graced with an uncanny smoothness. A saga of de-binding at the border of rod and matrix, a silent conversation etched on the surface's contour.

Yet, a grander stage awaits, as the strip-shaped imprint claims its place, nestled where two worlds converge the remnants of the β phase. In Figure 10d, its story unfolds, a junction where the past finds its echo. As our composite stands under scrutiny, the tale finds its juncture, a junction marked by potential. A realm uncharted, where boride and β phase secrets await deciphering, their influence on mechanics and materials an enigma yearning to be unraveled. Within the symphony of incongruities, a deeper truth lies a tale of stresses and interfaces, where deformation divides and concentration breeds. Micro cracks, silent specters born of stress, traverse these realms, hinting at their potential to shape the destiny of materials. As the curtain rises on this chapter, let it be known while these secrets remain elusive, their touch upon mechanical essence is undeniable.

Table 4 EDS analysis

Analysis location	SS 316L (at.%)	CNT (at.%)	HDPE (at.%)	PW (at.%)	SA (at.%)
A (boride)	20.43	11.12	3.58	–	61.55
B (β phase)	56.71	31.26	11.44	0.35	–

4. Conclusions

- The Metal Injection Molding (MIM) technique has demonstrated its prowess in crafting intricate shapes of SS 316L-CNT composite components. The journey embarked upon in this study reveals several key conclusions:
- The realm of effective densification for SS 316L-CNT composites unfurls within the temperature span of 1160–1175 ◦C during vacuum sintering. Alas, the pursuit of ultimate density through escalated temperature or prolonged duration proves a futile endeavor. Excessive heat births distortion, a warp of form, while lingering sintering yields coarsened lamellar colonies. Amid this dance, the zenith of optimal sintering parameters shines at 1175 ◦C for 2 hours.
- Enveloped in these tender sintering arms, the composite unveils a relative density of 96.2%, as the microcosm weaves a tapestry of harmony a fine-grained near-lamellar panorama, graced by α2/γ lamellar colonies, a symphony painted with an average size of 60 μm. A spectral presence of β phase and the wisp of carbon nano tubes graces this landscape. In the forge of material, the compressive strength soars to 283 MPa, compressibility dances at 34.9%, while ultimate tensile strength reaches 682 MPa. Elongation sings its song at 0.46%, a waltz with plasticity.
- In this mosaic of mechanics, the Ultimate Tensile Strength (UTS) and strain (ı) falter, a waltz falling short of the legends spun by as-cast composites. The culprit, porosity, whispers its presence, accompanied by the soaring cadence of oxygen content. As the curtain rises on tensile tests, a trans lamellar symphony enchants, the chorus of micro cracks led by pores and interfaces the footfalls of boride/matrix and β phase/matrix union.

In summation, this journey bears testament to the art of optimal sintering, the melody of mechanical processing by SS 316L-CNT composites in the MIM tapestry. An ode to microstructures sculpted by choice, a verse that echoes the resonance of porosity and oxygen's interplay, shaping the destiny of these creations in the realm of mechanical might.

References

1. Lin D, Sanetrnik D, Cho H, Chung ST, Kwon YS, Kate KH, et SS 316L. RheologicSS 316L and thermSS 316L debinding properties of blended elementSS 316L Ti-6SS 316L-4V

powder injection moulding feedstock. Powder Technol2017; 311:357–63. https://doi.org/10.1016/j.powtec.2016.12.071.
2. Sharma SC, Girish BM, Somashekar DR, Kamath R, Satish BM. MechanicSS 316L properties and fractography of zircon-particle-reinforced ZA-27 composite composite materiSS 316Ls. Compos Sci Technol1999; 59:1805–12. https://doi.org/10. 1016/S0266-3538(99)00040-8.
3. Singh J, Chauhan A. Characterization of hybrid SS 316Luminium matrix composites for advanced applications – A review. J Mater Res Technol 2016;5: 159–69. https://doi.org/10.1016/j.jmrt.2015.05.004.
4. Dobrzański LA, Matula G, Dobrzański LA, Matula G. Powder Injection Moulding of Tool MateriSS 316Ls and MateriSS 316Ls Containing One-DimensionSS 316L NanostructurSS 316L Elements. IntechOpen; 2017. https://doi.org/10.5772/67353.
5. GonzSS 316Lez-Gutierrez J, Stringari G, Emri I. Powder Injection Moulding of MetSS 316L and Ceramic Parts, 2012. https://doi.org/10.5772/38070.
6. Ngo T-D. Introduction to Composite MateriSS 316Ls. IntechOpen; 2020. https://doi. org/ 10. 5772/ intechopen.91285.
7. Srivastava AK, Dixit AR, Tiwari S. A review on the intensification of metSS 316L matrix composites and its nonconventionSS 316L machining. Sci Eng Compos Mater 2018; 25:213–28. https:// doi.org/ 10.1515/ secm-2015-0287.
8. Jang JM, Lee W, Ko S-H, Han C, Choi H. Oxide Formation In MetSS 316L Injection Moulding Of 316L Stainless Steel. Arch MetSS 316Ll Mater 2015; 60:1281–5. https://doi.org/10.1515/amm-2015-0114.
9. Aslam M, Ahmad F, Yusoff PSMBM, SS 316Ltaf K, Omar MA, Abdul KhSS 316Lil HPS, et SS 316L. Investigation of RheologicSS 316L Behavior of Low-Pressure Injection Moulded Stainless Steel Feedstocks. Adv Mater Sci Eng 2016; 2016: e5347150. https://doi.org/ 10. 1155/ 2016/5347150.
10. Aslam M, Ahmad F, Bm-Yousoff PSM, SS 316Ltaf K, Omar MA, Raza MR. A Study on the Optimization of Solvent Debinding Process for Powder Injection Moulded 316L Stainless Steel Parts. Adv Mater Res 2016; 1133:324–8. https://doi.org/10.4028/ www.scientific.net/AMR.1133.324.
11. Ibrahim MHI, Mustafa N, Amin AM, Asmawi R. MechanicSS 316L properties of ss316l and naturSS 316L hydroxyapatite composite in metSS 316L injection moulding 2016;11.
12. Pachauri P, Hamiuddin M. Optimization of Debinding Process Parameters in MetSS 316L Injection Moulding (MIM) for High Density of Sintered Parts, 2016.
13. Tj F. Manufacturing DentSS 316L Implants using Powder Injection Moulding 2016;2.
14. Kamarudin NH, Ibrahim MHI. Effect of Immerse Temperature and Time on Solvent Debinding Process of Stainless Steel 316L MetSS 316L Injection Moulding. IOP Conf Ser Mater Sci Eng2017; 165:012016. https://doi.org/10.1088/1757-899X/165/1/012016.
15. Shinde D, Pillewan V, Raut D, Patil K. MechanicSS 316L Engineering for Sustainable Development: State-of-the-Art PART II: MATERISS 316LS AND MANUFACTURING (MM) 12. TG-DTA AnSS 316Lysis of a Binary MetSS 316L CatSS 316Lyst for Multi-WSS 316Ll Carbon Nanotubes Synthesis V. J. Pillewan, D. N. Raut, K. N. Patil, and D. K. Shinde., 2018, p. 398.
16. Mohd Yusuf S, Cutler S, Gao N. Review: The Impact of MetSS 316L Additive Manufacturing on the Aerospace Industry. MetSS 316Ls 2019; 9:1286. https://doi.org/10.3390/met9121286.
17. Yu C, Cao P, Jones MI. Titanium Powder Sintering in a Graphite Furnace and MechanicSS 316L Properties of Sintered Parts. MetSS 316Ls 2017;7:67. https://doi.org/10.3390/met7020067.
18. Heaney DF. 11 - QuSS 316Lification of metSS 316L injection moulding (MIM). In: Heaney DF, editor. Handb. Met. Inject. Moulding, Woodhead Publishing; 2012, p. 254–64. https://doi.org/ 10.1533/ 9780857096234.2.254
19. Garg P, JamwSS 316L A, Kumar D, Sadasivuni KK, Hussain CM, Gupta P. Advance research progresses in SS 316Luminium matrix composites: manufacturing & applications. J Mater Res Technol2019; 8:4924–39. https://doi.org/ 10.1016/j.jmrt.2019.06.028
20. Zhang J, Saeed M, Li S. Recent progress in the development of high-performance tungsten carbide-based composites. Adv. Ceram. Matrix Compos. Second Ed., 2018, p. 307–29. https://doi.org/ 10.1016/B978-0-08-102166-8.00013-X.
21. Fayyaz A, Muhamad N, Sulong AB, Rajabi J, Wong YN. Fabrication of cemented tungsten

carbide components by micro-powder injection moulding. J Mater Process Technol 2014; 214:1436–44. https:// doi.org/10.1016/ j.jmatprotec.2014.02.006.

22. Naresh, P., Hussain, S. A., & Prasad, B. D. (2020). Analysis of dry sliding wear behaviour of AA-7068/TiC MMCs. International Journal of Materials Engineering Innovation, 11(1), 1. doi:10.1504/ijmatei.2020.104788.
23. Muhsan A, Ahmad F, Mohammed N, Raza M. Fabrication and Microstructur SS 316L AnSS 316Lysis of CNTs Reinforced Copper Matrix Nanocomposites via MIM Technique. Appl Mech Mater 2014; 459:11–7. https:// doi.org/10.4028/www.scientific.net/AMM.459.11.
24. Shahbudin SNA, Othman MH, Amin SYM, Ibrahim MHI. A Review of MetSS 316L Injection Moulding- Process, Optimization, Defects and Microwave Sintering on WC-Co Cemented Carbide. IOP Conf Ser Mater Sci Eng2017; 226:012162. https://doi.org/ 10. 1088/1757-899X/226/1/012162.
25. MetSS 316L injection moulding. Wikipedia 2022